Supporting Information

$AgBi(SO_4)(IO_3)_2$: Aliovalent Substitution Induces Structure Dimensional Upgrade and Second Harmonic Generation Enhancement

Hongming Liu[a,b,e], Qingchen Wu[c], Lili Liu[b,d], Zheshuai Lin,*[c] P. Shiv Halasyamani,*[b] Xingguo Chen*[a] and Jingui Qin[a]

[a] Hubei Key Laboratory on Organic and Polymeric Opto-electronic Materials, College of Chemistry and Molecular Sciences, Wuhan University, Wuhan 430072, China. E-mail: xgchen@whu.edu.cn

[b] Department of Chemistry, University of Houston, 112 Fleming Building, Houston, Texas 77204, USA. E-mail: psh@uh.edu

[c] Beijing Center for Crystal R&D, Technical Institute of Physics and Chemistry, Chinese Academy of Sciences Beijing 100190, China. E-mail: zslin@mail.ipc.ac.cn

[d] School of Materials Science and Engineering, Shanghai Institute of Technology, Shanghai 200235, China

[e] School of Chemistry and Chemical Engineering, Guangxi University, Nanning 530004, China.

Table of Contents

Experimental

Reagents. Ag_2O (Alfa Aesar, 99+%), Bi_2O_3 (Alfa Aesar, 99%), HIO_3 (Alfa Aesar, 99%), sulfuric acid (Alfa Aesar, 95.0-98.0%). All raw chemicals were purchased from Thermo Fisher Scientific Company and used without further treatment.

Synthesis. Raw materials of 0.5 mmol Ag_2O (0.1158 g), 0.5 mmol Bi_2O_3 (0.2329 g), 2 mmol HIO_3 (0.3518 g), 4 mL of distilled water, and 1 mL sulfuric acid were loaded in a 23 mL Teflon lines autoclave. The autoclave was closed, heated to 230 ^oC, and held for 4 days before cooled down to room temperature at a rate of about 2.7 ^oC/h. The product was filtered and washed with distilled water and ethanol. After drying, colorless block crystals (Figure 1) subsequently determined to be $AgBi(SO_4)(IO_3)_2$ (**ABSI**) were recovered with a yield of approximately 95% based on Bi. The purity of compound was been checked by powder X-ray diffraction (PXRD).

Powder X-ray diffraction. PXRD measurement was carried out on a PANalytical X'Pert PRO diffractometer with Cu-Kα radiation (λ=1.54186 Å) at 40 kV and 45 mA at room temperature. Crystal samples of **ABSI** were ground and scanned in the angular range of 2Θ =10^o-70^o with a step size of 0.008^o at a scanning rate of 3^o min^{-1}. As shown in Figure S1, the PXRD pattern matches well with the simulated data from the single-crystal structure.

Energy dispersive X-ray spectroscopy (EDX). EDX analyses were performed on an FEI Quanta 200 scanning electron microscope equipped with an energy dispersive X-ray spectrometer. An average molar ratio of approximately 0.87: 1: 1.22: 1.90 for Ag: Bi: S: I was found.

Single crystal structure determination. The crystal structure of **ABSI** was determined by single crystal X-ray diffraction. The data were collected at 296 K using a Bruker SMART APEX2 diffractometer equipped with a CCD detector (graphite-monochromated Mo Kα radiation, λ=0.71073 Å). The SAINT program was applied for data reduction and integration.[1] The structure was solved by direct methods and refined using the SHELXTL-97 software package.[2, 3] Relevant crystallographic data and structure refinement information for **ABSI** are summarized in Table 1, and its selected bond distances are listed in Tables S1-S3.

Infrared (IR) **spectroscopy.** The infrared spectrum from 4000-400 cm^{-1} for **ABSI** was recorded on a Thermo Scientific Nicolet iS10 FT-IR spectrometer at room temperature.

UV-vis-NIR Diffuse Reflectance Spectroscopy. The UV-vis diffuse reflectance spectrum was recorded on a Varian Cary 5000 UV-vis-NIR spectrophotometer equipped with an integrating sphere in the wavelength range of 200-1000 nm. The absorption spectrum was calculated from the reflectance spectrum using the Kubelka–Munk function: $\alpha/S = (1-R)^2/2R$, where α is the absorption coefficient, S is the scattering coefficient, and R is the reflectance, respectively.[4]

Thermogravimetric (TG) analysis. The TG analysis was carried out using an EXSTAR TG/DTA 6300 analyzer. Fine crystal samples of about 15 mg were added into a platinum crucible and heated from room temperature to 700 ^oC at a heating rate of 10 ^oC/min under a flowing nitrogen

atmosphere.

Second harmonic generation (SHG) measurement. The SHG measurement was carried out using the method of Kurtz and Perry[5] at 1064 nm and 1950 nm respectively. Polycrystalline samples of **ABSI** were ground and sieved into particle size ranges of 20-45, 45-63, 63-75, 75-90, 90-125, 125-145, 145-200 and 200-250 mm for the test. Similarly sieved microcrystalline KH_2PO_4 (KDP) and $KTiOPO_4$ (KTP) served as the standard.

First-principle calculations. First-principle calculations were conducted using the CASTEP software[6], a plane-wave pseudopotential package based on density functional theory (DFT)[7]. The exchange-correlation energy was described by the generalized gradient approximation (GGA)[8] scheme of Perdew−Burke−Ernzerhof (PBE) functional.[9] Norm-conserving pseudopotentials[10] (Ag $4s^2 4p^6 4d^{10} 5s^1$, Bi $5d^{10} 6s^2 6p^3$, I $5s^2 5p^5$, O $2s^2 2p^4$, S $3s^2 3p^4$) were employed to simulate the ion-electron interactions. A kinetic energy cutoff of 850 eV and Monkhorst-Pack[11] *k*-point meshes (5×4×2) spanning less than 0.04/Å^3 in the Brillouin zone were chosen. Before calculating electronic structure and optical properties, the atomic positions in the unit cell were fully optimized using BFGS[12] method, while the cell parameters were fixed. Due to the discontinuity of exchange-correlation, band gaps calculated by the GGA method are usually smaller than experimental values. Therefore, a scissors operator[13] was adopted to raise the conduction bands to match the experimental value. Using the scissors-corrected electronic structure, the SHG coefficients were calculated using an expression developed by Lin *et al*.[14] To further evaluate the contributions of relevant groups to SHG effect, an SHG-weighted electron density analysis[15] was performed.

Table S1. Crystallographic data and structure refinement for **ABSI**.

Formula	$Ag_2Bi_2(SO_4)_2(IO_3)_4$
FW	1525.42
Space group	Triclinic, *P*1
a(Å)	5.5189(4)
b(Å)	6.9129(4)
c(Å)	11.8527(8)
α(°)	90.5980(10)
β(°)	92.1510(10)
γ(°)	109.8950(10)
Volume(Å^3)	424.78(5)
Z	1
D_{calcd} (Mg/m^3)	5.963
Absorption coefficient (mm^{-1})	30.546
F(000)	664
Crystal size(mm^3)	0.020×0.020×0.020
GOF on F^2	1.065
Flack parameter	0.095(5)
R_1/wR_2 [I>2σ(I)]	0.0368/0.0905
R_1/wR_2 (all data)	0.0368/0.0905
$R_1=\Sigma\|\|F_o\|-\|F_c\|\|/\Sigma\|F_o\|$ and $wR_2=[\Sigma w(F_o^2-F_c^2)^2/\Sigma wF_o^4]^{1/2}$ for $F_o^2>2\sigma(F_o^2)$	

Table S2. Atomic coordinates ($\times 10^4$), equivalent isotropic displacement parameters ($Å^2 \times 10^3$), and BVC for **ABSI**. U(eq) is defined as one third of the trace of the orthogonalized U^{ij} tensor.

Atom	x	y	z	U(eq)	BVC
Ag(1)	1836(3)	304(2)	9316(2)	18(1)	1.00
Ag(2)	5926(3)	8511(3)	7321(2)	18(1)	1.02
Bi(1)	35(1)	5908(1)	4939(1)	9(1)	3.02
Bi(2)	4886(1)	6247(1)	464(1)	9(1)	3.11
I(1)	2542(2)	2028(2)	6583(1)	9(1)	5.18
I(2)	-572(2)	5348(2)	8123(1)	7(1)	4.87
I(3)	-2063(2)	2285(2)	915(1)	7(1)	4.89
I(4)	6566(2)	9883(2)	4456(1)	6(1)	4.97
O(1)	2530(30)	4650(20)	6458(13)	20(3)	1.99
O(2)	40(30)	1140(20)	7577(12)	17(3)	2.18
O(3)	5110(30)	2330(20)	7603(13)	21(3)	1.95
O(4)	-970(30)	6570(20)	6810(11)	18(3)	2.23
O(5)	2590(30)	7140(20)	8626(11)	14(3)	2.19
O(6)	-2380(30)	6640(20)	8906(11)	13(3)	2.30
O(7)	560(20)	3790(20)	42(12)	15(3)	2.04
O(8)	-4650(20)	3051(19)	257(11)	10(2)	2.33
O(9)	-2730(30)	-50(20)	84(12)	13(2)	2.17
O(10)	3970(20)	8470(20)	5385(11)	9(2)	2.24
O(11)	9060(20)	9100(20)	5093(11)	11(2)	2.17
O(12)	7300(20)	12260(20)	5279(11)	13(3)	1.99
O(13)	1690(30)	3380(20)	3969(12)	16(3)	1.74
O(14)	5980(30)	5860(20)	3804(12)	19(3)	1.71
O(15)	3120(20)	4640(20)	2135(11)	11(2)	1.93
O(16)	5010(30)	2380(20)	3076(12)	17(3)	1.55
O(17)	1560(20)	7640(20)	3209(11)	11(2)	1.87
O(18)	2710(20)	8750(20)	1324(11)	13(3)	1.84
O(19)	-1450(20)	6300(20)	1599(11)	13(3)	1.87
O(20)	-520(30)	9760(20)	2276(12)	17(3)	1.60
S(1)	3970(8)	4039(7)	3244(4)	7(1)	5.84
S(2)	594(8)	8163(7)	2110(4)	7(1)	5.97

Table S3. Bond lengths [Å] for **ABSI**.

Bond	Lengths	Bond	Lengths
Ag(1)-O(2)	2.415(14)	Bi(2)-O(6)#7	2.389(12)
Ag(1)-O(8)#1	2.430(13)	Bi(2)-O(7)	2.442(14)
Ag(1)-O(5)#2	2.498(15)	Bi(2)-O(9)#3	2.503(13)
Ag(1)-O(9)	2.645(17)	Bi(2)-O(18)	2.638(14)
Ag(1)-O(18)	2.715(14)	Bi(2)-O(5)#8	2.662(13)
Ag(1)-O(6)	2.819(12)	I(1)-O(3)	1.784(14)
Ag(1)-O(3)	2.822(15)	I(1)-O(2)	1.799(13)
Ag(1)-O(7)	2.864(15)	I(1)-O(1)	1.821(15)
Ag(2)-O(2)#3	2.381(15)	I(2)-O(6)	1.818(12)
Ag(2)-O(5)	2.397(13)	I(2)-O(4)	1.820(13)
Ag(2)-O(10)	2.495(13)	I(2)-O(5)	1.834(14)
Ag(2)-O(4)#4	2.593(13)	I(3)-O(9)	1.801(14)
Ag(2)-O(6)	2.611(15)	I(3)-O(8)	1.833(11)
Ag(2)-O(1)	2.842(12)	I(3)-O(7)	1.833(13)
Ag(2)-O(3)	2.844(16)	I(4)-O(11)	1.790(12)
Bi(1)-O(10)	2.325(13)	I(4)-O(12)	1.816(14)
Bi(1)-O(4)	2.383(13)	I(4)-O(10)	1.846(12)
Bi(1)-O(17)	2.417(13)	S(1)-O(13)	1.495(13)
Bi(1)-O(11)#5	2.446(13)	S(1)-O(14)	1.492(15)
Bi(1)-O(12)#6	2.504(14)	S(1)-O(15)	1.490(13)
Bi(1)-O(13)	2.515(15)	S(1)-O(16)	1.461(14)
Bi(1)-O(14)#5	2.560(14)	S(2)-O(17)	1.485(13)
Bi(1)-O(1)	2.561(14)	S(2)-O(18)	1.470(13)
Bi(2)-O(8)#4	2.322(13)	S(2)-O(19)	1.498(13)
Bi(2)-O(15)	2.357(13)	S(2)-O(20)	1.451(14)
Bi(2)-O(19)#4	2.377(13)		

Table S4. Band gaps of some reported bismuth-containing iodates

Formula	Eg (eV)	Formula	Eg (eV)
$Bi_2(IO_4)(IO_3)_3$[16]	3.3	$Bi_2Te(IO_3)O_5Cl$[17]	3.6
$BiO(IO_3)$[18]	3.3	$KBi_2(IO_3)_2F_5$[19]	3.75
$K_2BiI_5O_{15}$[20]	3.50	$RbBi_2(IO_3)_2F_5$[19]	3.78
$Rb_2BiI_5O_{15}$[20]	3.53	$CsBi_2(IO_3)_2F_5$[19]	3.84
$Bi_3OF_3(IO_3)_4$[21]	3.7	$(NH_4)Bi_2(IO_3)_2F_5$[22]	3.88
$Bi(IO_3)F_2$[23]	3.97	$KBi(IO_3)_3(OH)$ [24]	3.50
$Bi_2O(SeO_4)(IO_3)_2$[25]	3.70	$NaBi(IO_3)_4$[24]	3.45
$Bi_2O(SO_4)(IO_3)_2$[25]	3.74	$AgBi(SO_4)(IO_3)_2$	3.40

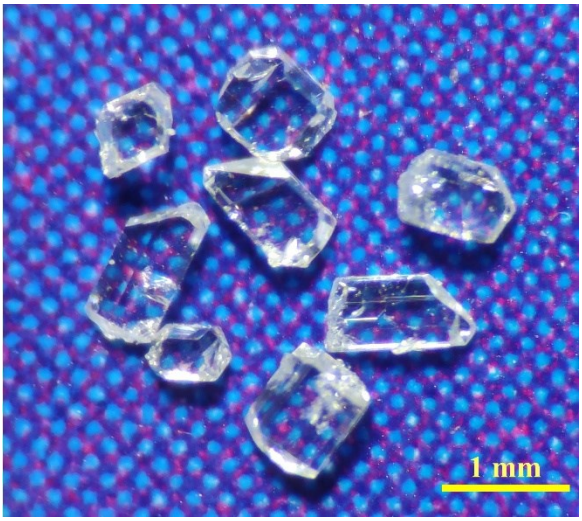

Figure S1 The image of single crystals of **ABSI**.

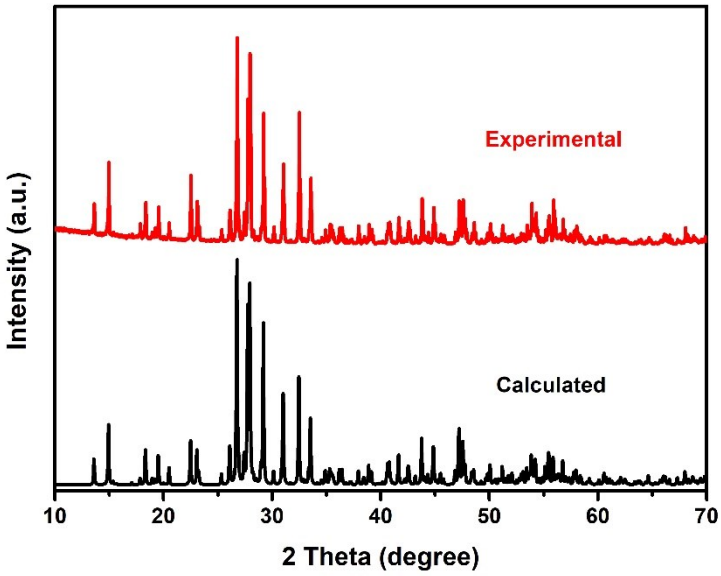

Figure S2. Simulated and measured powder X-ray diffraction patterns of **ABSI**

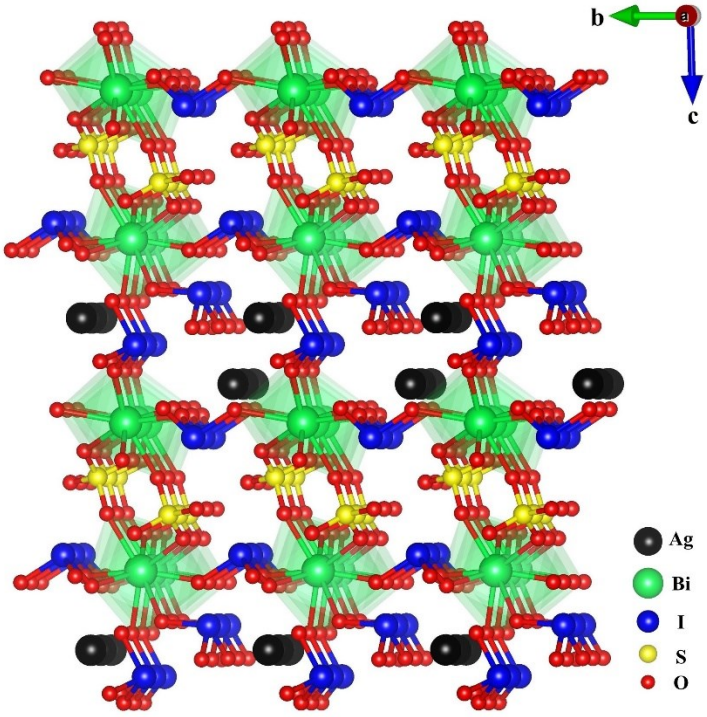

Figure S3. The three-diensional structure of **ABSI**

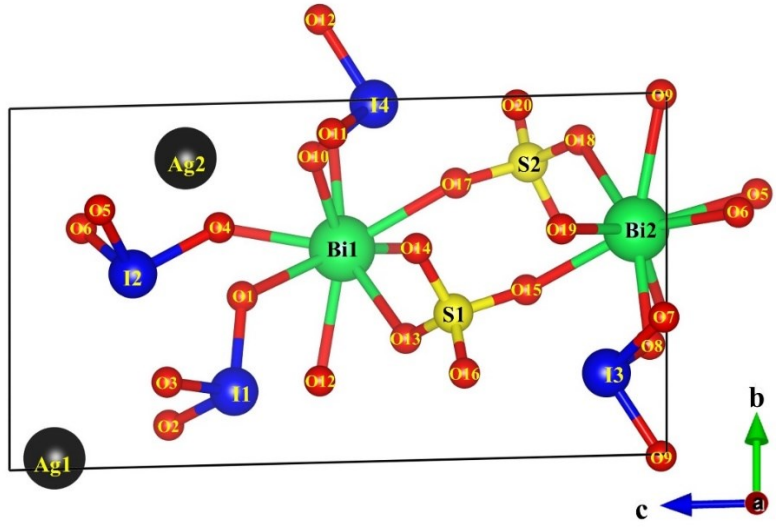

Figure S4. The unit cell of **ABSI**

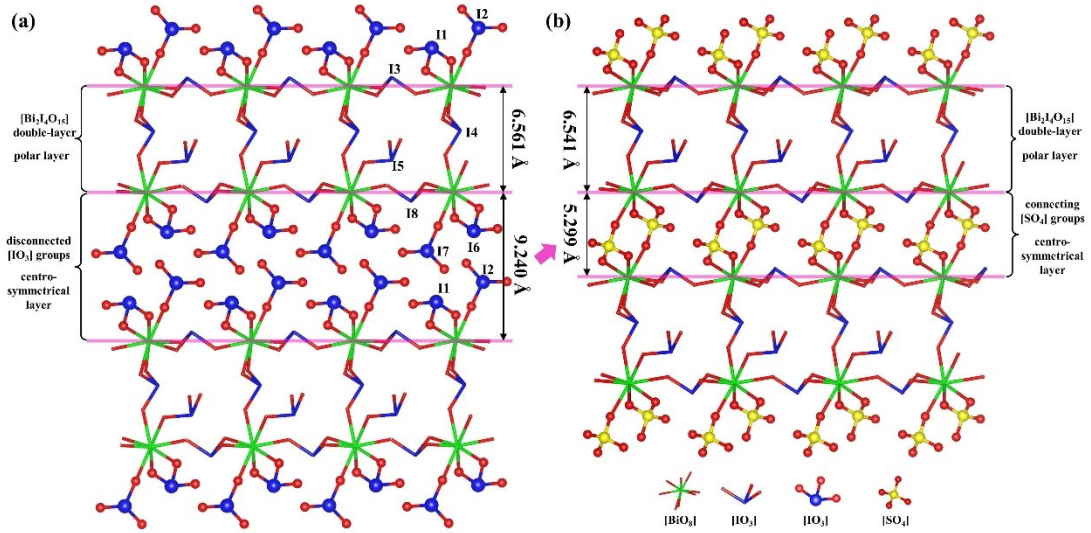

Figure S5. The framework of (a) $AgBi(IO_3)_4$ (**ABI**) and (b) $AgBi(SO_4)(IO_3)_2$ (**ABSI**) (with Ag atoms removed). The polar $[Bi_2I_4O_{15}]$ doube-layer formed by $[BiO_8]$ and $[IO_3]$ are in the wires mode. And centro-symmetrical layers consisting by $[I(1)O_3]$, $[I(2)O_3]$, $[I(6)O_3]$, $[I(7)O_3]$ groups in **ABI** and $[SO_4]$ groups in **ABSI** on both sides of polar layer are in the ball-and-stick mode.

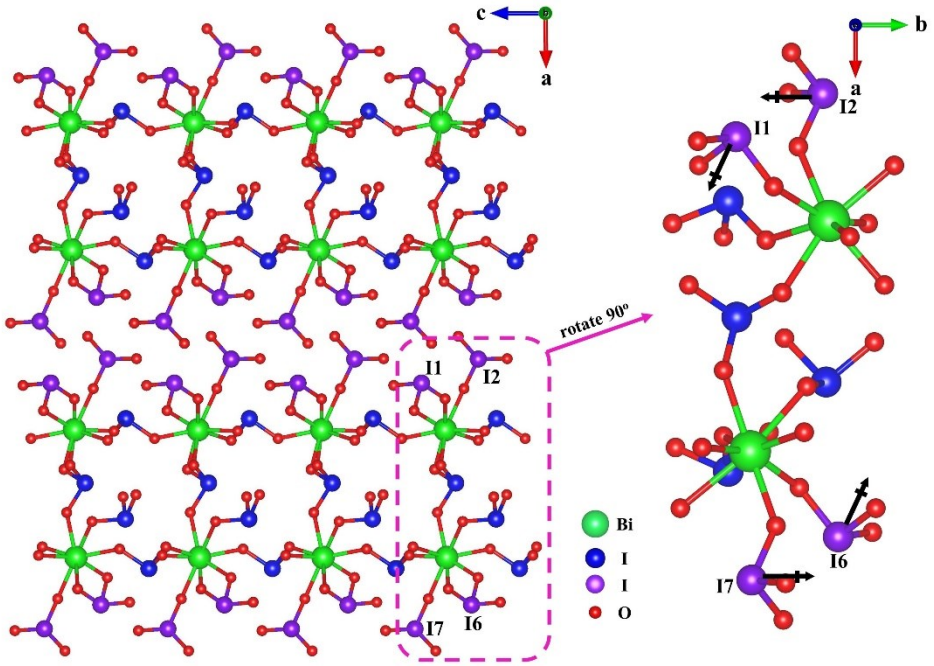

Figure S6. The approximate local dipole moment (black arrow) for $[IO_3]$ groups on both sides of $[Bi_2I_4O_{15}]_\infty$ layer in the structure of $AgBi(IO_3)_4$. They are connected by centro-symmetry operation with local dipole moment canceling each other out.

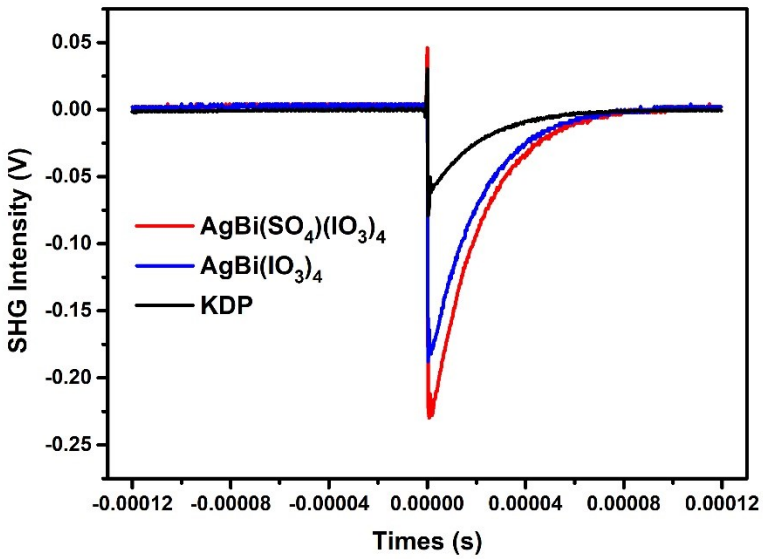

Figure S7. Oscilloscope traces of the SHG signals for KDP, **ABI** and **ABSI** at the powder size of 200–250 μm under 1064 nm laser radiation

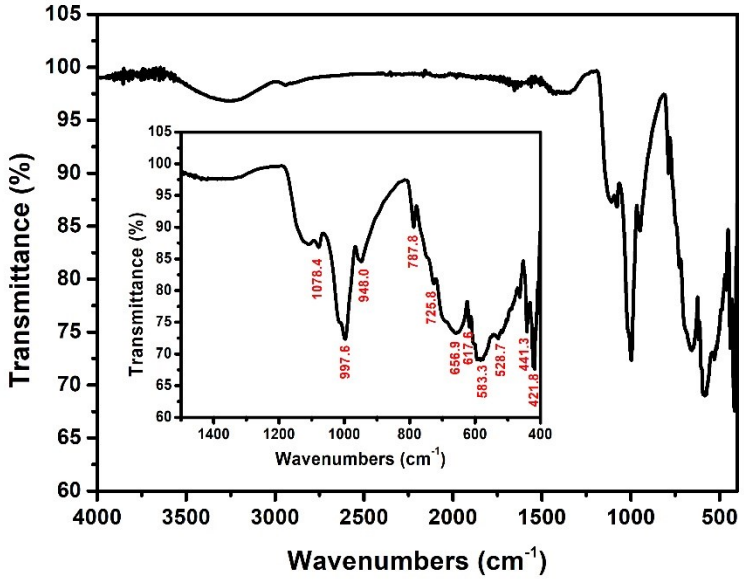

Figure S8. The IR spectrum of **ABSI**

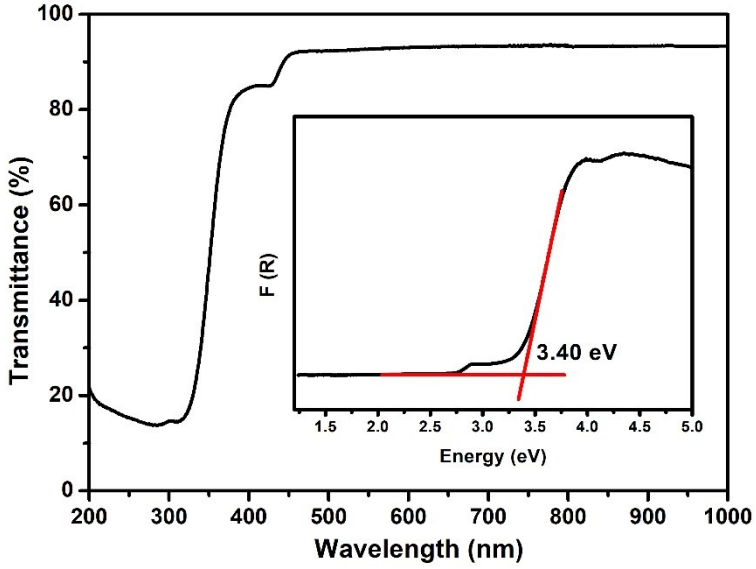

Figure S9. The UV-vis diffuse reflectance spectrum of **ABSI**

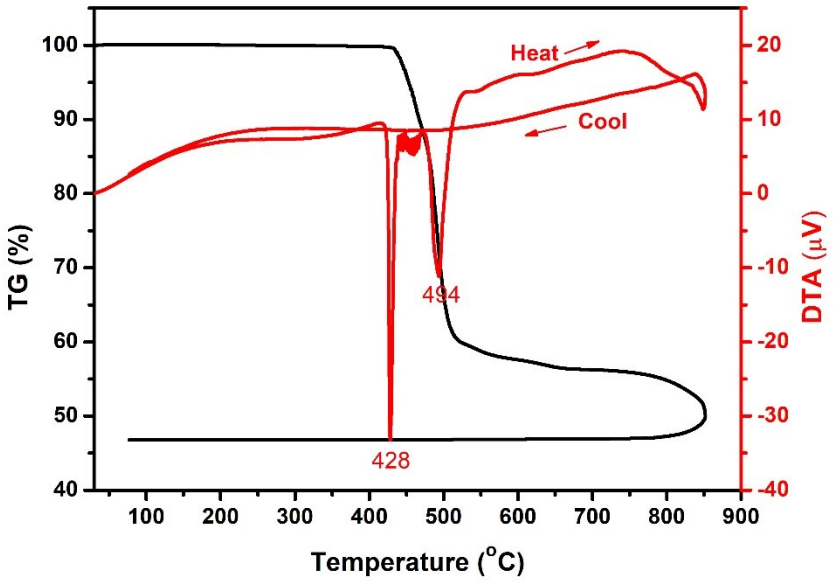

Figure S10. TG and DTA curves for **ABSI**

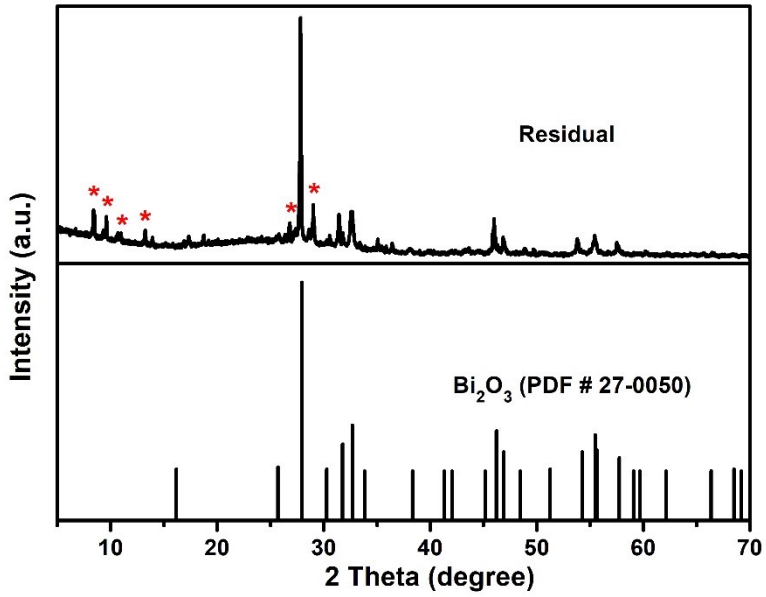

Figure S11. The powder XRD patterns of the residue after TG analysis of **ABSI** (some unknown peaks are labeled by red stars)

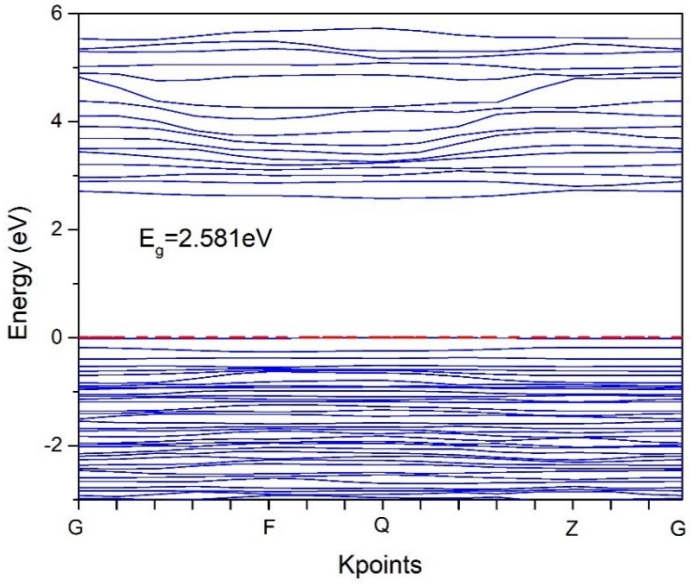

Figure S12. The calculated electron band structures of **ABSI**

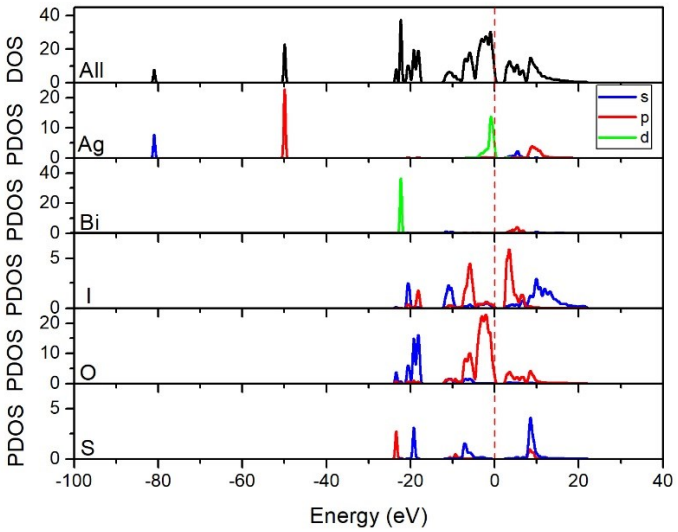

Figure S13. The partial density of states (PDOS) projected onto the constituent atoms of **ABSI**

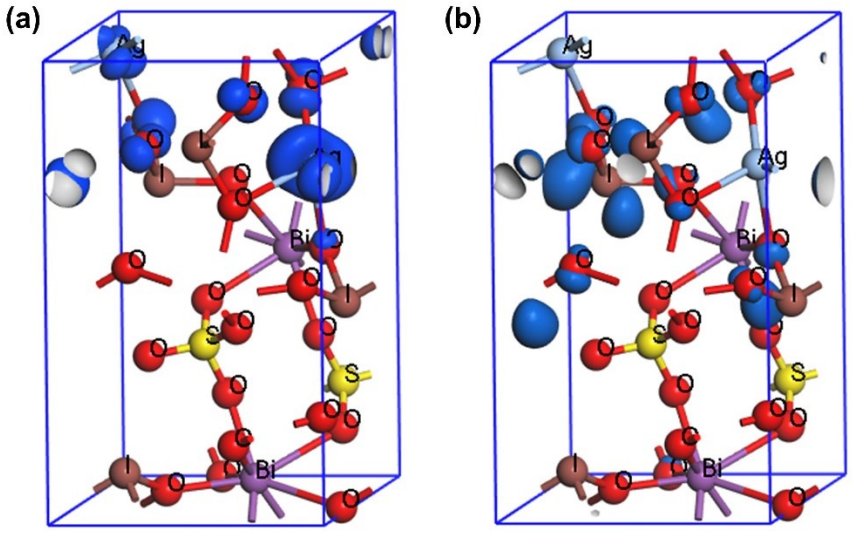

Figure S14. The orbital isosurfaces showing the highest orbital under VB maximum (a) and the lowest orbital above CB minimum (b) in **ABSI**

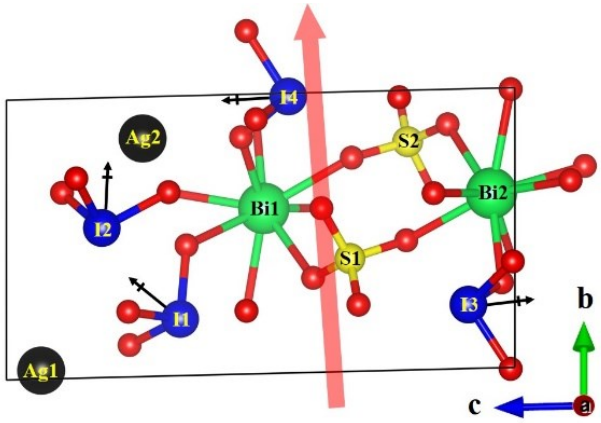

Figure S15. The approximate local dipole moment (black arrow) for [IO_3] groups and net-polarization (red arrow) in the unit cell of **ABSI**

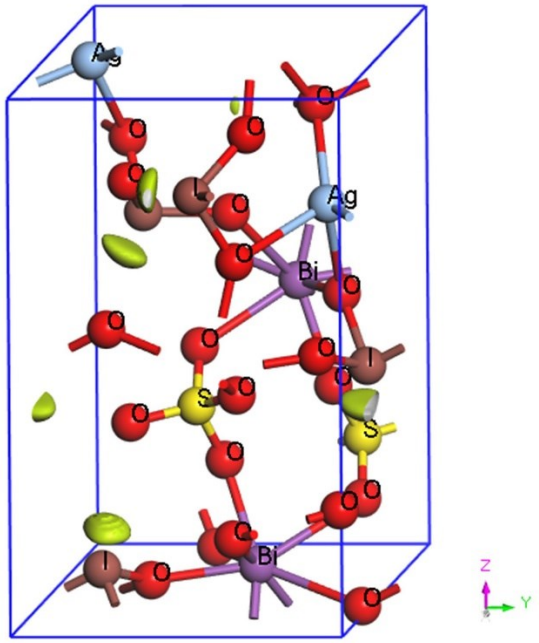

Figure S16. The electron localization function (ELF) isosurfaces for the pseudopotential calculations of **ABSI**

REFERENCES

1. V. SAINT, *Inc., Madison, WI*, 2008.
2. G. M. Sheldrick, *Acta Crystallographica Section A*, 2008, **64**, 112-122.
3. G. M. Sheldrick, *Inc.: Madison, WI*, 2003.
4. W. M. Wendlandt and H. G. Hecht, *Reflectance spectroscopy: Interscience*, J Wiley and Sons, Inc., New York, 1966.
5. S. K. Kurtz and T. T. Perry, *J. Appl. Phys.*, 1968, **39**, 3798-3813.
6. S. J. Clark, M. D. Segall, C. J. Pickard, P. J. Hasnip, M. I. Probert, K. Refson and M. C. Payne, *Zeitschrift für Kristallographie*, 2005, **220**, 567-570.
7. W. Kohn and L. J. Sham, *Phys. Rev.*, 1965, **140**, A1133-A1138.
8. J. P. Perdew, K. Burke and M. Ernzerhof, *Phys. Rev. Lett.*, 1996, **77**, 3865-3868.
9. J. P. Perdew and Y. Wang, *Phys. Rev. B*, 1992, **46**, 12947-12954.
10. A. M. Rappe, K. M. Rabe, E. Kaxiras and J. D. Joannopoulos, *Phys. Rev. B*, 1990, **41**, 1227-1230.
11. H. J. Monkhorst and J. D. Pack, *Phys. Rev. B*, 1976, **13**, 5188-5192.
12. B. G. Pfrommer, M. Côté, S. G. Louie and M. L. Cohen, *J. Comput. Phys.*, 1997, **131**, 233-240.
13. R. W. Godby, M. Schlüter and L. J. Sham, *Phys. Rev. B*, 1988, **37**, 10159-10175.
14. J. Lin, M. Lee, Z. Liu, C. Chen and C. J. Pickard, *Phys. Rev. B*, 1999, **60**, 13380-13389.
15. M. Lee, C. Yang and J. Jan, *Phys. Rev. B*, 2004, **70**, 235110.
16. Z. Cao, Y. Yue, J. Yao, Z. Lin, R. He and Z. Hu, *Inorg. Chem.*, 2011, **50**, 12818-12822.
17. L. Geng, C. Meng, H. Lu, Z. Luo, C. Lin and W. Cheng, *Dalton Trans.*, 2015, **44**, 2469-2475.
18. S. D. Nguyen, J. Yeon, S. Kim and P. S. Halasyamani, *J. Am. Chem. Soc.*, 2011, **133**, 12422-12425.
19. H. Liu, Q. Wu, X. Jiang, Z. Lin, X. Meng, X. Chen and J. Qin, *Angew. Chem. Inter. Ed.*, 2017, **129**, 9620-9624.
20. Y. Huang, X. Meng, P. Gong, L. Yang, Z. Lin, X. Chen and J. Qin, *J. Mater. Chem. C*, 2014, **2**, 4057-4062.
21. M. Zhang, X. Su, M. Mutailipu, Z. Yang and S. Pan, *Chem. Mater.*, 2017, **29**, 945-949.
22. H. Fan, C. Lin, K. Chen, G. Peng, B. Li, G. Zhang, X. Long and N. Ye, *Angew. Chem. Inter. Ed.*, 2020, **132**, 5306-5310.
23. F. Mao, C. Hu, X. Xu, D. Yan, B. Yang and J. Mao, *Angew. Chem. Inter. Ed.*, 2017, **56**, 2151-2155.
24. Y. Jia, Y. Chen, T. Wang, Y. Guo, X. Guan and X. Zhang, *Dalton Trans.*, 2019, **48**, 10320-10326.
25. L. Shi, D. Mei, J. Xu and Y. Wu, *Solid State Sci.*, 2017, **63**, 54-61.